Molecular Biology of the Cell
Vol. 17, 4937–4945, December 2006

Tracking of Quantum Dot-labeled CFTR Shows Near Immobilization by C-Terminal PDZ Interactions[D] [V]

Peter M. Haggie,* Jung Kyung Kim,* Gergely L. Lukacs,† and A. S. Verkman*

*Departments of Medicine and Physiology, University of California, San Francisco, San Francisco, CA 94143-0521; and †Hospital for Sick Children Research Institute, Toronto, Ontario M5G 1X8, Canada

Submitted August 3, 2006; Accepted September 6, 2006
Monitoring Editor: Vivek Malhotra

Mutations in cystic fibrosis transmembrane conductance regulator (CFTR), a cAMP-regulated chloride channel, cause cystic fibrosis. To investigate interactions of CFTR in living cells, we measured the diffusion of quantum dot-labeled CFTR molecules by single particle tracking. In multiple cell lines, including airway epithelia, CFTR diffused little in the plasma membrane, generally not moving beyond 100–200 nm. However, CFTR became mobile over micrometer distances after 1) truncations of the carboxy terminus, which contains a C-terminal PDZ (PSD95/Dlg/ZO-1) binding motif; 2) blocking PDZ binding by C-terminal green fluorescent protein fusion; 3) disrupting CFTR association with actin by expression of a mutant EBP50/NHERF1 lacking its ezrin binding domain; or 4) skeletal disruption by latrunculin. CFTR also became mobile when the cytoskeletal adaptor protein binding capacity was saturated by overexpressing CFTR or its C terminus. Our data demonstrate remarkable and previously unrecognized immobilization of CFTR in the plasma membrane and provide direct evidence that C-terminal coupling to the actin skeleton via EBP50/ezrin is responsible for its immobility.

INTRODUCTION

The relatively common genetic disease cystic fibrosis is caused by mutations in the cystic fibrosis transmembrane conductance regulator (CFTR) gene. The CFTR protein is a cAMP-regulated chloride channel expressed in plasma membranes of many epithelial cell types in the airways/lung and gastrointestinal and reproductive tracts. CFTR is a polytopic glycoprotein (1480 amino acids) containing at its cytoplasm-facing surface two nucleotide binding domains, a regulatory domain, and its N and C termini. There has been considerable interest in interaction of postsynaptic density protein 95/discs large/zonula occludens-1 (PSD95/Dlg/ZO-1; PDZ) domain proteins at the CFTR C terminus (amino acid residues DTRL), which forms a consensus class I PDZ binding domain (C-terminal X-[S/T]-X-[V/I/L]; Wang *et al*., 1998). The C terminus of CFTR was initially shown to interact with ezrin-radixin-moesin (ERM) binding phosphoprotein of 50 kDa (EBP50; alternative name NHERF1, Na^+/H^+ exchanger regulatory factor 1), which has been proposed to tether CFTR to the actin cytoskeleton through ezrin and possibly other proteins (Figure 1A) (Hall *et al*., 1998; Short *et al*., 1998; Wang *et al*., 1998; Guggino and Stanton, 2006). The C terminus of CFTR has also been demonstrated to interact with the PDZ domain proteins NHERF2/E3KARP (Sun *et al*., 2000b), CAP70/PDZK1 (Wang *et al*., 2000), and CAL/GOPC/FIG/PIST (Cheng *et al*., 2002).

Several unrelated roles for CFTR–PDZ interactions have been proposed, including apical polarization/targeting (Moyer *et al*., 1999a, 2000), plasma membrane recycling (Swiatecka-Urban *et al*., 2002), direct regulation of CFTR channel gating (Wang *et al*., 2000; Raghuram *et al*., 2001, 2003; Benharouga *et al*., 2003), and assembly or trafficking of CFTR–protein complexes with β2-adrenergic receptors (Naren *et al*., 2003) and Kir 1.1 K^+ channels (Yoo *et al*., 2004). Several controversies exist; for example, although the CFTR C terminus was initially demonstrated to mediate apical polarization (Moyer *et al*., 1999a, 2000), subsequent work in multiple cell culture models reported that polarization is not affected by C-terminal mutations (Benharouga *et al*., 2003; Ostedgaard *et al*., 2003). In other systems, PDZ interactions are involved in protein polarization/retention (e.g., of epidermal growth factor receptor 2; Shelly *et al*., 2003), stabilization/degradation (e.g., of β2-adrenergic receptor; Cao *et al*., 1999), and regulation of function (e.g., of Na^+/H^+ exchanger; Weinman *et al*., 1995).

Reduced CFTR diffusional mobility is predicted if CFTR–EBP50–ezrin–actin interactions are relatively stable and involve the majority of CFTR molecules at the plasma membrane. We previously used fluorescence recovery after photobleaching to investigate plasma membrane diffusion of CFTR tagged with green fluorescent protein (GFP) at its N terminus (Haggie *et al*., 2004). Diffusion of most CFTR molecules was fairly rapid and unrestricted and increased ~50% after C-terminal deletion/mutation. Similarly, in a recent study, CFTR labeled with streptavidin-conjugated fluorophores were largely (50–60%) mobile by photobleaching and image correlation spectroscopy (Bates *et al*., 2006). Here, to study CFTR mobility and interactions at the single molecule level, we performed time-lapse imaging and single

This article was published online ahead of print in *MBC in Press* (http://www.molbiolcell.org/cgi/doi/10.1091/mbc.E06–08–0670) on September 20, 2006.

[D] [V] The online version of this article contains supplemental material at *MBC Online* (http://www.molbiolcell.org).

Address correspondence to: Alan S. Verkman (alan.verkman@ucsf.edu).

Abbreviations used: CFTR, cystic fibrosis transmembrane conductance regulator; EBP50, ezrin-radixin-moesin (ERM) binding phosphoprotein of 50 kDa; PDZ, postsynaptic density protein 95/discs large/zonula occludens-1 (PSD95/Dlg/ZO-1); Qdots, quantum dots; SPT, single particle tracking.

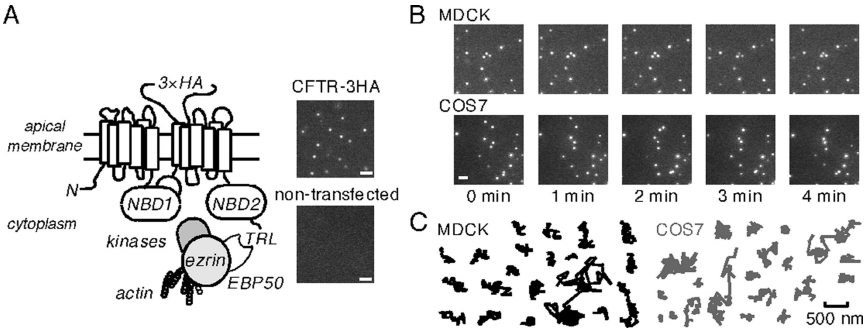

Figure 1. Time-lapse imaging of CFTR in the plasma membrane. (A) Schematic of CFTR showing its C-terminal PDZ binding domain, along with NHERF1/EBP50, ezrin, kinases, and the actin cytoskeleton. Inset, fluorescence micrographs of COS7 cells expressing CFTR-3HA (top) and nontransfected control cells (bottom) labeled with anti-HA antibody, biotin Fab fragment, and streptavidin-conjugated Qdots. Bar, 2 μm. (B) Image sequence for Qdot-labeled CFTR-3HA in MDCK epithelia and COS7 cells. Time of individual frames is indicated. Bar, 2 μm. (C) Representative trajectories (over 5 min) for CFTR-3HA expressed in indicated cell lines. Bar applies to all trajectories.

particle tracking (SPT) of quantum dot-labeled CFTR molecules. The bright, stable fluorescence of quantum dots (Qdots), and their minimal interactions with membranes permitted tracking of CFTR molecules with nanometer-scale resolution and near zero background signal. Measurements were done using several mammalian cell lines expressing an externally epitope-tagged CFTR, including primary cultures of human airway epithelium, allowing direct visualization of plasma membrane CFTR at very low membrane density as found in native, CFTR-expressing cells. Appropriate processing, plasma membrane stability, internalization and recycling of externally tagged CFTR have been verified previously (Sharma *et al*., 2004; Pedemonte *et al*., 2005). Contrary to initial expectations, we found dramatic immobilization of wild-type CFTR, which was largely accounted for by coupling of its C terminus to the actin skeleton via PDZ domain binding proteins.

MATERIALS AND METHODS

cDNA Constructs, Cell Culture, and Transfection

Plasmids encoding CFTR with a triplet hemagglutinin (3HA) epitope tag inserted in the fourth extracellular loop of wild-type human CFTR (CFTR-3HA), CFTR lacking 26 (CFTR-3HA-Δ26), or 70 (CFTR-3HA-Δ70) C-terminal amino acids, and with a GFP fused to the C terminus after the PDZ-binding motif (CFTR-3HA-GFP) have been described previously (Benharouga *et al*., 2003; Sharma *et al*., 2004; Pedemonte *et al*., 2005). Plasmids encoding GFP fused to the C-terminal 87 amino acids of CFTR (GFP-CFTRct87) and the CFTR C-terminal region without the PDZ binding motif (GFP-CFTRct87Δ6) were generated in pEGFP-C1 (Clontech, Mountain View, CA) by using standard procedures. GFP chimeras of EBP50 (GFP-EBP50) and EBP50 mutated to remove the C-terminal ezrin binding domain (GFP-EBP50ΔEBD) have also been described previously (Haggie *et al*., 2004).

Cells were grown at 37°C in a 5% CO_2/95% air atmosphere. Standard conditions were used to culture COS7, HT29, and Calu-3 cells lines. Human bronchial epithelial (HBE) cells were isolated and primary cultures were grown as described previously (Widdicombe *et al*., 2003). Baby hamster kidney (BHK) cells stably expressing CFTR-3HA were grown in DMEM H21/Ham's F-12 supplemented with 5% fetal bovine serum (FBS), 100 U/ml penicillin, 100 μg/ml streptomycin, and 500 μM methotretate (Haardt *et al*., 1999; Benharouga *et al*., 2003). Madin-Darby canine kidney type II (MDCK II) epithelial cells were infected with virus expressing CFTR-3HA by incubating cells in viral supernatant supplemented with 8 μg/ml polybrene for 12 h. Infected cells were selected in the presence of 1 mg/ml G418 (Geneticin; Invitrogen, Carlsbad, CA), and cells were maintained in DMEM-H21 containing 10% FBS, 100 U/ml penicillin, 100 μg/ml streptomycin, and 1 mg/ml G418. To generate virus stocks, CFTR-3HA was subcloned into the retroviral expression cassette pFBneo (Stratagene, La Jolla, CA), and virus was generated by transient cotransfection of human embryonic kidney 293 (HEK 293) cells with the pVpack GP and pVpack VSVG packaging plasmids (Stratagene). An MDCK cell line stably expressing CFTR with an N-terminal GFP moiety has been described previously (Moyer *et al*., 1999a; Haggie *et al*., 2004). Transient transfection were performed with Lipofectamine 2000 (Invitrogen; COS7, BHK, and MDCK) and JetPEI (Polyplus-Transfection, San Marco, CA; HBE and HT29) according to the manufacturers' instructions.

Quantum Dot Labeling and Cell Treatments

Single particle tracking experiments were performed on confluent cells grown on 18-mm coverglasses that were transfected 1–3 d before experiments; enriched cell populations were plated 2–4 d before experiments. Cells were blocked (phosphate-buffered saline [PBS] containing 6 mM glucose, 1 mM pyruvate, and 1% bovine serum albumin [BSA]; 5 min) and labeled by sequential room temperature incubations with 0.05–0.1 μg/ml anti-HA antibody (HA.11 mouse monoclonal antibody; Covance, Princeton, NJ) for 5–7 min, with 0.05–0.1 μg/ml goat anti-mouse biotin-SP-conjugated AffiniPure Fab fragment (Jackson ImmunoResearch Laboratories, West Grove, PA) for 5–7 min, and with 0.1 nM streptavidin-conjugated Qdots (Invitrogen) for 2 min in PBS containing 6 mM glucose and 1 mM pyruvate (PBS gluc/pyr). Qdots emitting at 605 nm were used, except that 655-nm Qdots were used when GFP chimeras were expressed. Cells were washed with PBS gluc/pyr three times between incubations and 6–10 times after Qdot incubations. Fab fragments were generated from the anti-HA antibody using the ImmunoPure Fab preparation kit (Pierce Biotechnology, Rockford, IL), confirmed to be pure by reductive SDS-PAGE and used at 0.1–0.3 μg/ml for 5 min. Goat anti-mouse IgG AffiniPure Fab fragment conjugated with Cy3 (Jackson ImmunoResearch Laboratories) was used to label anti-HA Fab fragments at 0.15 μg/ml for 2–5 min.

For SPT measurements, coverglasses containing labeled cells were mounted in a custom chamber, and temperature was maintained at 37°C during experiments. The following cell treatments were used: latrunculin (0.5–2 μM; 5–10 min), jasplakinolide (2.5 μM; 5 min), forskolin (20 μM; 5 min), CPT-cAMP (100 μM; 5 min), and phorbol 12-myristate 13-acetate (PMA; 0.2 μM; 10 min), with compounds included in the bathing solution during tracking measurements and during labeling. Cells fixation was done with paraformaldehyde (4% in PBS; 10 min) immediately after labeling. In some experiments, CFTR expression was increased by culturing cells in medium containing 5 mM sodium butyrate for 16–24 h before experiments. For all maneuvers, data were obtained from 8 to 27 cell regions using at least duplicate coverslips. To generate a population of endocytosed/internalized Qdot-labeled CFTR molecules, labeled cells were incubated at 37°C for 2 h, and Qdots remaining at the cell surface were removed by an acid wash (2 min; PBS titrated to pH 2 with HCl; Groc *et al*., 2004). Biotinylated lipid [*N*-(biotinoyl)-1,2-dihexadecanoyl-*sn*-glycero-3-phosphoethanolamine, biotin DHPE; Invitrogen] was incorporated into cell plasma membranes by incubation for 30 min in PBS gluc/pyr containing 1% BSA and liposomes (40 μM lipid) generated by ethanol/chloroform evaporation of a 80:20 M mix of 1-palmitoyl-2-oleoyl-*sn*-glycerol-3-phosphocholine and biotin DHPE lipid. Plasma membrane biotin-DHPE was subsequently labeled by incubation of cells with 0.1 nM Qdots for 2 min.

Single Particle Tracking

Single particle tracking was done on a Nikon Eclipse TE2000U inverted microscope equipped with an Exfo X-Cite light source, Nikon 100× (numerical aperture 1.45) total internal reflection fluorescence oil immersion objective, Hamamatsu EM-charge-coupled device deep-cooled camera and Uniblitz shutter. Qdot fluorescence was excited using 420/40x excitation filter and 470DCXR dichroic mirror, and fluorescence was detected through 605/40m or 655/40m emission filters (Chroma Technology, Brattleboro, VT). In GFP-chimera expression experiments, cells were initially visualized using a GFP filter set (Chroma Technology). Data were obtained within 10 min of the final wash step after cell labeling (with acid washing used to quantify the fraction of Qdots remaining at the cell surface). Single particle tracking was generally done using continuous 100-ms acquisitions for 1 min. The spatial resolution of the system, defined as the ability to determine the centroid of a fluorophore (rather than optical diffraction limit) was ~10 nm at 10 frames per second (fps) as measured by the standard deviation of centroid coordinates for immobilized Qdots (Fujiwara *et al*., 2002). In some experiments, images were obtained for 5 min at 0.9 fps by using 200-ms image acquisition time and shuttered illumination light.

Data Analysis

Individual TIF images were extracted from sequence files and recompiled as 8-bit image stacks by using ImageJ (National Institutes of Health, Bethesda,

MD). Image analysis and trajectory construction were performed using IDL software (Research Systems, Boulder, CO) with algorithms available as shareware at http://www.physics.emory.edu/faculty/weeks/. Intermittency of Qdot fluorescence was used to verify that single fluorophores were analyzed, and extracted trajectories were at least 4 s in length.

For each trajectory, mean square displacement (MSD), $\langle r^2(t)\rangle$, was computed as follows:

$$\langle r^2(n\delta t)\rangle = \frac{1}{N-n}\sum_{j=0}^{N-n-1}\{[x(j\delta t + n\delta t) - x(j\delta t)]^2 + [y(j\delta t + n\delta t) - y(j\delta t)]^2\} \quad (n = 0, 1, 2, \ldots, N-1) \quad (1)$$

where δt is the temporal resolution of the acquisition device, $(x(j\delta t), y(j\delta t))$ is the particle coordinate at time $t = j\delta t$, and N is the total number of frames recorded for an individual particle. Offsets in MSD curves because of the uncertainty in fluorophore centroid position were corrected, and individual MSD versus time curves were fitted using the Levenberg–Marquardt nonlinear least squares fitting algorithm, to a cut-off time of $N/4$ (Saxton, 1997) by using a combined quadratic, polynomial and exponential function (with fitting parameters a_1, a_2, and a_3) given by the following:

$$\langle r^2(t)\rangle_{fit} = a_1t^2 + a_2[1 - \exp(-a_3t)] \qquad (0 \le t \le t_{cut\text{-}off}) \quad (2)$$

The microscopic diffusion coefficient, $D_{1\text{-}3}$, was computed by linear squares fitting by using points 1–3 on the MSD curve: $D_{1\text{-}3} = \langle r^2(t)\rangle_{1\text{-}3}/8\delta t$. The range of particle diffusion at time t_F was computed as range $= [\langle r^2(t_F)\rangle_{fit}]^{1/2}$. For immobile particles (defined as MSD less than or equal to the positional accuracy of the system), D and range were assigned values of 0 $\mu m^2/s$ and 0 μm, respectively, for histogram plotting.

Immunoblotting and Immunohistochemistry

Western blot analysis of CFTR expression levels was performed using the M3A7 anti-CFTR antibody at 1:1000 dilution as described previously (Sharma *et al.*, 2004). To determine surface expression of CFTR-3HA cells were washed in PBS, blocked (PBS with 1% BSA for 5 min at 4°C), and incubated with 1 μg/ml Alexa Fluor 488-conjugated anti-HA antibody (Invitrogen) for 20 min at 4°C. Cells were then washed, fixed, and imaged to determine background-subtracted cell area-integrated fluorescence intensity.

RESULTS

The diffusion of CFTR molecules was studied using an engineered CFTR containing an external epitope tag. Figure 1A shows a schematic of the expressed CFTR with a triple HA tag inserted into its fourth extracellular loop. Also shown are the putative interacting proteins EBP50 and ezrin, and the actin cytoskeleton. Figure 1A (right top) shows bright, particulate labeling of live CFTR-3HA–expressing COS7 cells after successive incubations with anti-HA antibody, biotin-conjugated Fab fragment, and streptavidin-conjugated Qdots, with nontransfected COS7 cells showing ~1% labeling (right bottom). Selective Qdot labeling of the epitope-tagged CFTR was verified in all cell types studied, with ~1–2% nonspecific labeling in nontransfected cells.

To assess the long-term mobility of CFTR in the plasma membrane of live cells, we performed time-lapse imaging of Qdot-labeled CFTR at ~1 Hz over 5 min. A representative image sequence is shown in Figure 1B (top) for MDCK epithelial cells expressing CFTR-3HA and labeled with Qdots (Supplemental Video 1). Visual inspection of the image sequence indicated that CFTR moved little over 5 min, with only ~10% of Qdots moving more than ~500 nm. Examples of Qdot trajectories are shown in Figure 1C (left) for CFTR-3HA in MDCK cells, which endogenously express EBP50 and ezrin (Short *et al.*, 1998; Bretscher *et al.*, 2002; Naren *et al.*, 2003). To verify confined CFTR diffusion in other cell systems, CFTR-3HA was expressed in COS7 fibroblasts (which also express EBP50 and ezrin [Figure 1B, bottom, and Supplemental Video 2]). CFTR diffusion was similarly confined in COS7 (Figure 1C, bottom right) and MDCK cells.

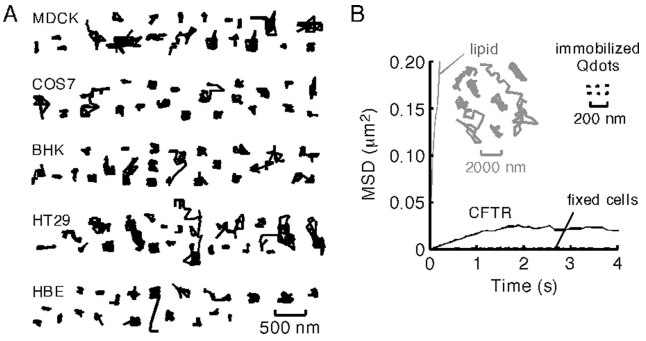

Figure 2. Single particle tracking of CFTR. (A) Representative trajectories of CFTR-3HA diffusion in the plasma membrane of kidney (MDCK), colon (HT29), and HBE, and in COS7 and BHK fibroblasts. Trajectories were acquired at 10 fps; each trajectory ~6 s in duration. Bar applies to all trajectories. (B) MSD versus time plots for CFTR-3HA in control (solid line) and paraformaldehyde-fixed (dashed line) cells, and for Qdot-labeled lipid (inset). Trajectories of immobilized Qdots and Qdot-labeled lipid shown for comparison (note different length scales). MSD plots are averaged from four to six cells.

Whereas time-lapse imaging provides descriptive information about long-term CFTR mobility, the relatively slow frame rate precludes quantitative determination of diffusion coefficients (D) and diffusion mechanisms. As such, we carried out SPT at 10 frames per second on Qdot-labeled CFTR-3HA expressed in a several cell lines. In agreement with the results in Figure 1, Figure 2A shows remarkably confined CFTR-3HA diffusion in cell lines, including kidney (MDCK), colonic (HT29), and human bronchial epithelial (HBE) cells (Supplemental Videos 3 and 4). Individual trajectories (over 6 s) generally did not extend beyond a radius of 100–200 nm. MSD plots derived from trajectories of CFTR-3HA expressed in COS7 cells showed downward curvature, indicating confined CFTR diffusion (Figure 2B), with similar MSD plots for the other cell types (data not shown). The deduced mean D value for short-range CFTR motions of mobile CFTR-3HA was $\sim 5 \times 10^{-11}$ cm^2/s (0.005 $\mu m^2/s$), in the range found for other membrane proteins, but with a high degree of confinement. The MSD plot for paraformaldehyde-fixed cells showed an even greater degree of confinement (Figure 2B, dashed line), indicating that CFTR diffusion in nonfixed cells, albeit highly confined, was nonzero. For comparison, trajectories from Qdots immobilized on a glass surface are shown (acquired with the same parameters and used to determine the optical precision of the system) as well as those for Qdot-labeled membrane lipids (Figure 2B, inset), which show remarkably greater diffusion than CFTR.

To verify that the labeling procedure did not restrict CFTR mobility, we performed control experiments with Fab fragments generated from the anti-HA antibody. Diffusive behavior of CFTR-3HA labeled with Fab fragments versus full antibody was essentially identical (Supplemental Figure S1, A). Additionally, CFTR-3HA trajectories derived from cells labeled with anti-HA Fab fragment and Cy3-conjugated secondary Fab fragment (instead of Qdots) showed similar confinement (Supplemental Figure S1, B), indicating that Qdot labeling cannot be responsible for CFTR confinement. Also, as presented below, Qdot-labeled CFTR became mobile after various mutations and maneuvers. Finally, control studies were done to validate the sampling rate of 10 fps used in this study. Data were collected at higher frame rates of 30 fps (video rate) and 60 fps (Supplemental Figure S1, C). The distributions of D and range for CFTR, and a mutant

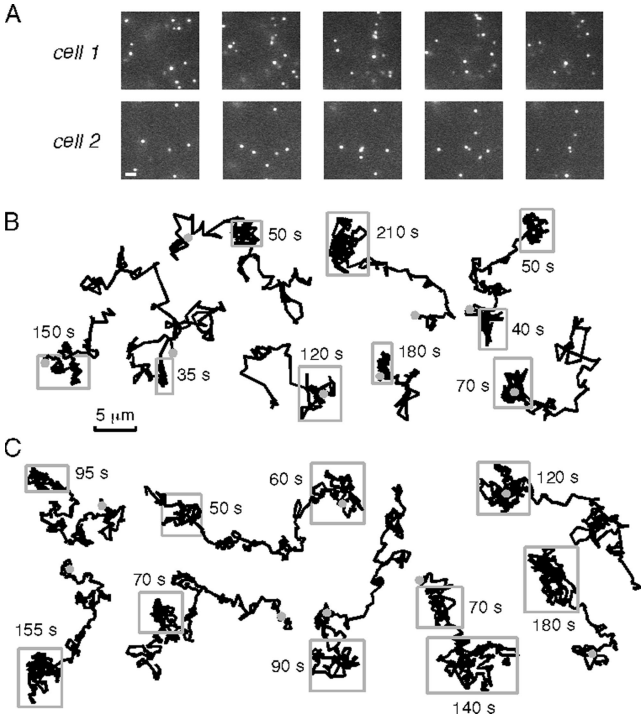

Figure 3. Time-lapse imaging of CFTR with truncated C terminus. (A) Image sequences for Qdot-labeled CFTR-3HA-Δ26 expressed in COS7 cells. Time of individual frames is indicated. Bar, 2 μm. (B) Representative trajectories over 5 min, with gray circles indicating start points. Rectangles shown over some regions of trajectories along with time interval remaining in box. (C) Representative trajectories for simulated random Brownian diffusion (without confinement), with single diffusion coefficient chosen to mimic experimental data in B. Rectangles shown (from visual inspection) as in B. See text for explanations.

CFTR with faster diffusion, were essentially identical at 10, 30, and 60 fps, indicating the adequacy of image collection for the measurements here.

To investigate the role of the CFTR C terminus in its confined diffusion, we performed time-lapse imaging of a naturally occurring CFTR mutant that lacks its C terminus PDZ binding motif (CFTR-3HA-Δ26; Benharouga *et al.*, 2003). Experiments were done in COS7 cells that express EBP50 (Naren *et al.*, 2003) but that do not express endogenous CFTR that could confound interpretation through possible interactions with the mutant-transfected protein. Figure 3A shows representative image sequences of CFTR-3HA-Δ26; ~70% of the mutant CFTR was mobile, with many mutant CFTR molecules moving over micrometer distances (Supplemental Video 5). Representative trajectories shown in Figure 3B indicates remarkably less confinement than that seen for wild-type CFTR-3HA, but it suggests the possibility of transient confinement as indicated by the boxed regions in many of the trajectories. From similar trajectories, a recent study concluded that a different CFTR mutant lacking PDZ-type interactions diffused between zones of transient confinement (Bates *et al.*, 2006). However, further analysis of our data revealed that regions of apparent confinement in Qdot trajectories do not represent bone fide confinement zones. Figure 3C shows simulated trajectories for simple (non-anomalous) diffusion without confinement, with a single diffusion coefficient chosen to mimic the range of trajectories seen experimentally. Visual inspection revealed qualitatively similar regions of apparent confinement as seen in the experimental data, suggesting that such regions represent statistical fluctuations rather than confinement zones. This finding was confirmed by a histogram analysis of apparent "confinement times," Δt_c, which showed similar distributions for the experimental Qdot data and the simulated data for simple diffusion, with very different Δt_c seen for simulated diffusion with zones of confinement (data not shown).

Single particle tracking at 10 fps was done to quantify the role of the CFTR C terminus (Figure 4). Additional trajectories for CFTR-3HA diffusion in COS7 cells are shown in the first panel of Figure 4A, with the averaged MSD versus time plot for many trajectories in the second panel. Panels 3 and 4 show histograms of "instantaneous" D (panel 3) and diffusive "range" (range, $MSD^{1/2}$ at 2 s, panel 4). As expected from visual inspection of trajectories, the distributions of D and range are relatively small, with ~17% of trajectories being completely immobile. A full analysis of the diffusive behavior of CFTR-3HA expressed in two other cell lines (BHK and MDCK cells) revealed similar marked confinement (Supplemental Figure S1, A, bottom).

Similar Qdot tracking experiments were done for two naturally occurring C-terminal CFTR deletions (removal of 26 amino acids, CFTR-3HA-Δ26, Figure 4B; and 70 amino acids, CFTR-3HA-Δ70, Figure 4C) and a C-terminal addition (CFTR with a C-terminal GFP after the PDZ binding domain, CFTR-3HA-GFP, Figure 4D) (also see Supplemental Video 6 showing CFTR-3HA-Δ70 diffusion). These C terminus modifications disrupt CFTR interactions with its PDZ domain binding partner EBP50 (Hall *et al.*, 1998; Moyer *et al.*, 1999a; Benharouga *et al.*, 2003). Compared with CFTR-3HA, the C-terminal deletions and addition caused remarkable mobilization of CFTR as seen in representative individual trajectories (Figure 4, B–D, first panels) and relatively linear MSD versus time plots to 4 s (second panels). Histograms from a large series of trajectories are summarized in Figure 4, A–D (panels 3 and 4). Whereas a narrow distribution of D was found for CFTR-3HA, much wider distributions in D were observed for the C-terminal deletions as well as increased range of CFTR diffusion.

We next studied the roles of EBP50 and actin in the membrane immobilization of CFTR. COS7 cells were cotransfected with CFTR-3HA and GFP chimeras of EBP50 or a dominant-negative EBP50 mutant with a C-terminal truncation that prevents ezrin binding (EBP50ΔEBD). Coexpression of GFP-EBP50 and CFTR-3HA yielded trajectories and diffusive characteristics (Figure 5A) showing significant confinement, as observed in cells with endogenous expression of EBP50. However, cotransfection with GFP-EBP50ΔEBD greatly increased CFTR-3HA mobility (Figure 5B), producing wider distributions of D and range. With GFP-EBP50ΔEBD expression, the histograms suggest the presence of both confined and mobile subpopulations of diffusing CFTR-3HA. Similar mobilization of CFTR by GFP-EBP50ΔEBD was found in MDCK and BHK cells stably expressing CFTR-3HA (data not shown). Treatment with latrunculin B, which fragments the actin cytoskeleton (Okamoto *et al.*, 2004), also increased CFTR-3HA D and range (Figure 5C), as did treatment of MDCK and BHK cells expressing CFTR-3HA (data not shown).

Treatment of cells expressing CFTR-3HA-Δ26 with jasplakinolide to increase the proportion of polymerized/stabilized actin had no significant effect on CFTR-3HA-Δ26 diffusion, suggesting that CFTR–actin interactions are predominantly mediated by the CFTR C terminus (Figure 5D). Membrane receptors with greater mobility that interact with the actin cytoskeleton are immobilized by jasplakinolide treatment (our unpublished observations), as expected be-

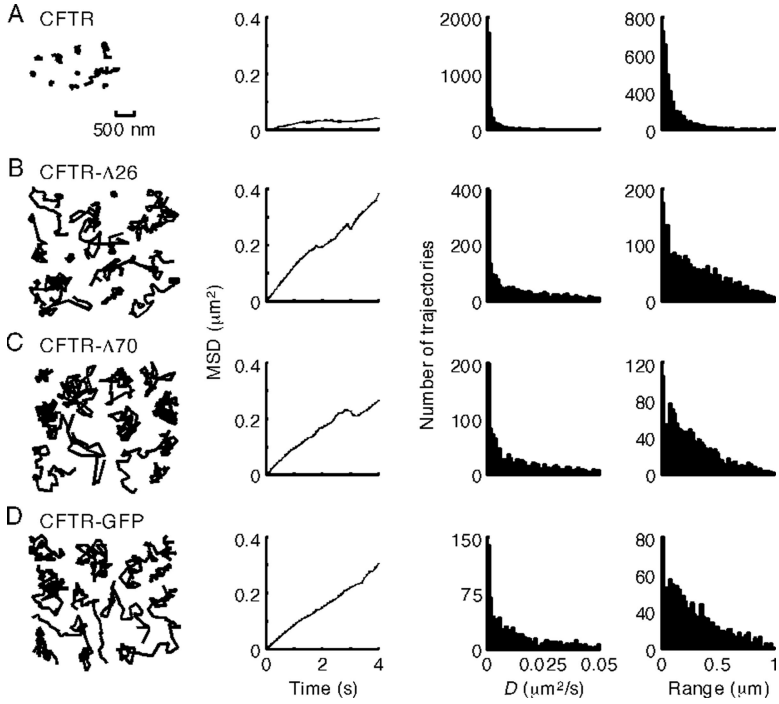

Figure 4. Increased CFTR mobility after truncation of its C terminus or blocking its C terminus by GFP fusion. Representative trajectories (first panel), MSD versus time plots (second panel), and histograms for the distributions of *D* (third panel) and range (at 2 s; fourth panel) for CFTR-3HA (A), CFTR-3HA-Δ26 (B), CFTR-3HA-Δ70 (C), and CFTR-3HA-EGFP (D) expressed in COS7 cells. Bar applies to all trajectories; data acquired at 10 fps. See text for explanation of characterization of diffusive properties. MSD versus time plots are averages of four to six individual cells.

cause jasplakinolide produces actin stabilization and immobilization (Okamoto *et al*., 2004).

CFTR is constitutively internalized by endocytosis (Prince *et al*., 1999; Bertrand and Frizzell, 2003; Sharma *et al*., 2004). The rate of CFTR internalization was estimated by Qdot labeling, 10 min chase at 37°C, and imaging before and after acid washing. For CFTR-3HA and CFTR-3HA-Δ26 in COS7 cells, there was 13 ± 2 and 16 ± 2% internalization at 10 min (7–8 cells studied; mean ± SE), slightly lower than reported previously (Sharma *et al*., 2004). As expected, endocytosed CFTR was essentially immobile over the time course of data acquisition (data not shown). Thus, endocytosis introduces minimal uncertainty in assignment of immobilized CFTR trajectories because all image acquisitions were done within 10 min after labeling. With single particle tracking, on average, ~8% of CFTR-3HA-Δ26 is immobilized because of endocytosis during data acquisitions; because ~20% of total CFTR-3HA-Δ26 trajectories were immobile (Figure 4B), only ~12% of CFTR-3HA-Δ26 was immobile owing to interactions mediated by CFTR domains other than the C terminus.

Stimulation of CFTR Cl^- channel function by protein kinase A with 100 μM CPT-cAMP or 20 μM forskolin or by

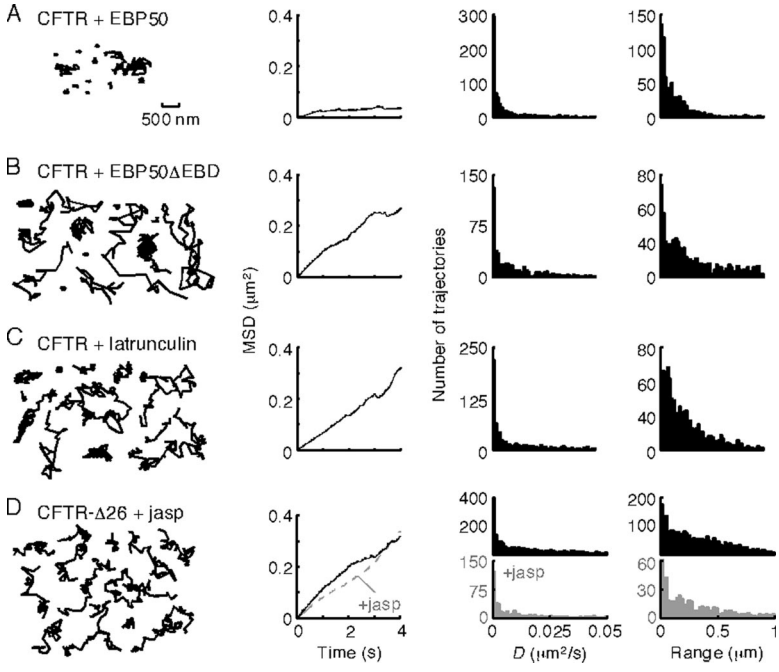

Figure 5. Role of NHERF1/EBP50 and actin in CFTR diffusion. Representative trajectories (first panels), MSD versus time plots (second panel), and distributions of *D* (third panel) and range (at 2 s; fourth panel) for COS7 cells expressing CFTR-3HA after GFP-EBP50 transfection (A), GFP-EBP50ΔEBD transfection (B), and latrunculin B treatment (0.5 μM; 10 min) (C). (D) Comparison of CFTR-Δ26 mobility in untreated cells (black; data as in Figure 2B) and after treatment with jasplakinolide (gray; 2.5 μM, 5 min). Data were acquired at 10 fps. Bar applies to all trajectories.

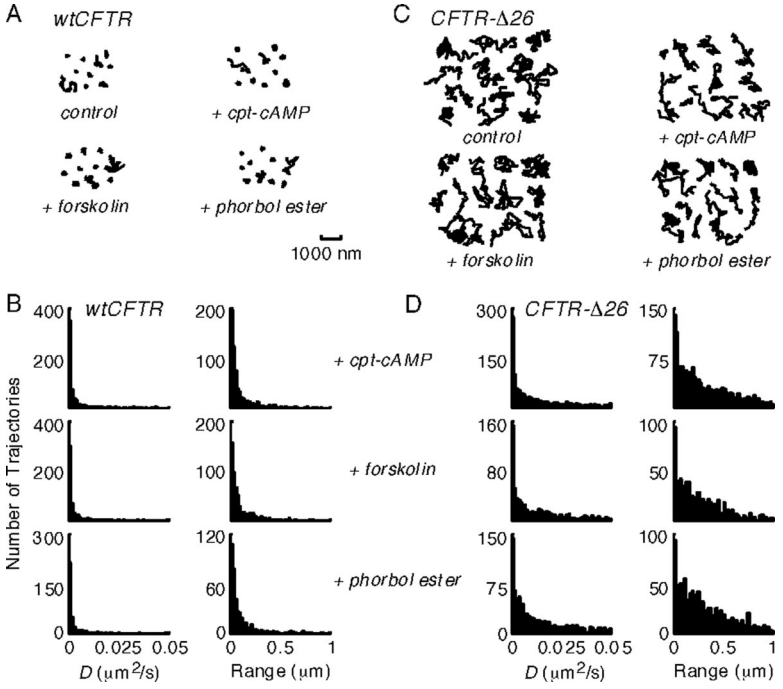

Figure 6. Effect of phosphorylation on CFTR diffusion. (A and C) Representative trajectories for COS7 cells expressing CFTR-3HA (A) and CFTR-3HA-Δ26 (C) under control conditions and after stimulation with CPT-cAMP, forskolin, and phorbol ester. Data were acquired at 10 fps. Bar applies to all trajectories. (B and D) Summary of diffusive characteristics for CFTR-3HA (B) and CFTR-3HA-Δ26 (D).

protein kinase C with 0.2 μM phorbol ester, did not affect CFTR-3HA mobility in COS7 cells (Figure 6, A and B). Also, phosphorylation of CFTR-3HA-Δ26 did not change its diffusive properties (Figure 6, C and D), indicating that CFTR phosphorylation does not affect its association with other proteins in a manner that alters its diffusion.

The above studies indicate that CFTR is highly confined in the plasma membrane in nonpolarized cells and epithelia and that its confinement involves C-terminal interactions with EBP50, ezrin, and actin. The finding of highly confined CFTR diffusion is quantitatively dissimilar to previous photobleaching measurements on GFP-CFTR chimeras (Haggie *et al.*, 2004) or externally labeled CFTR (Bates *et al.*, 2006), where CFTR diffused over micrometer distances. A fundamental difference between the Qdot tracking study here and the photobleaching measurements was the need to express significantly more GFP-CFTR (by butyrate stimulation) in the photobleaching study to obtain adequate signal for imaging.

To investigate whether the CFTR expression level could be responsible for the relatively free GFP-CFTR diffusion found by photobleaching, we treated COS7 cells expressing CFTR-3HA with 5 mM sodium butyrate overnight. In cells labeled in an identical manner with antibody, biotinylated Fab fragment and streptavidin Qdots, butyrate stimulation resulted in greatly increased surface CFTR expression (Figure 7A, inset). Quantitative image analysis of CFTR-3HA–transfected COS7 cells immunostained with Alexa Fluor 488-conjugated anti-HA antibody indicated an ~12-fold increase in CFTR surface expression by butyrate treatment, similar to the 25-fold increased in GFP-CFTR expression reported in butyrate-treated MDCK cells (compared with untreated GFP-CFTR–expressing cells) as used in the photobleaching study (Moyer *et al.*, 1999b). Figure 7A shows that CFTR-3HA overexpression produced by butyrate treatment produced clear-cut mobilization of a significant fraction of CFTR molecules, which we propose results from uncoupling of overexpressed CFTR from its binding partners (data acquired using 10% of the usual anti-HA antibody concentration to label only a fraction of surface CFTR). Figure 7B shows a comparison of the distributions of *D* and range for CFTR-3HA under control conditions (black histograms) and after butyrate stimulation (gray histograms), demonstrating increased CFTR mobility in high-expressing cells. For reference, the 50th percentile values (Q_2) and 75th percentile (Q_3) values are indicated. Single particle tracking done on low-expressing cells treated with 5 mM sodium butyrate for 5 min before and during the measurements showed confined diffusion, as in untreated cells, indicating that butyrate itself does not acutely alter CFTR diffusion (data not shown). We verified that the amount of CFTR-3HA expressed in the transfected cells studied here was similar to that in cells that endogenously express CFTR. Immunostaining with a fluorescently conjugated antibody indicated that cells transiently transfected with CFTR-3HA (COS7) or stably expressing CFTR-3HA (BHK and MDCK) had similar levels of CFTR at the plasma membrane (data not shown). Immunoblot analysis indicated that the CFTR-3HA–expressing cells had much less CFTR than Calu-3 cells but much more than HT29 cells (Figure 7B, inset), suggesting that the cells studied here had physiologically appropriate levels of CFTR expression.

To further test whether increased CFTR expression can causes its mobilization, CFTR-3HA was expressed in the MDCK epithelial cells used previously to measure GFP-CFTR mobility by photobleaching (Haggie *et al.*, 2004). Figure 7C shows that CFTR-3HA became mobile in butyrate-treated MDCK cells that overexpress GFP-CFTR. Finally, to verify that the amount of CFTR C termini (as opposed to alternative effects such as altered membrane fluidity or other CFTR domains) was responsible for the increased mobility of CFTR-3HA, soluble chimeras of GFP and the C terminus of CFTR (CFTRct87) were expressed. COS7 cells coexpressing CFTR-3HA and GFP-CFTRct87 chimera showed increased CFTR mobility (Figure 7D). In contrast, CFTR mobility was not increased in cells coexpressing CFTR-3HA and a GFP chimera containing a mutated CFTR C terminus lacking its PDZ binding domain (GFP-CFTRct87Δ6; data

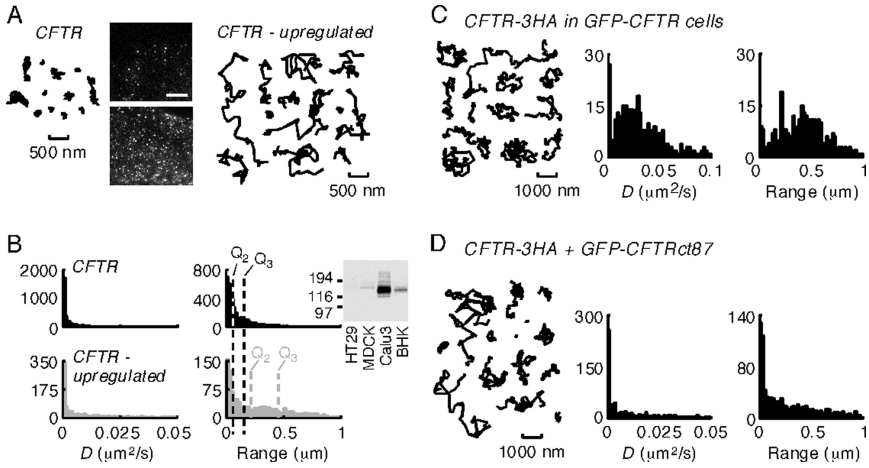

Figure 7. CFTR overexpression greatly increases its diffusion. (A) Representative trajectories of COS7 cells transiently transfected with CFTR-3HA before (left) and after (right) treatment with 5 mM sodium butyrate for 24 h. Fluorescence micrographs of COS7 cells expressing CFTR-3HA shown as insets with Qdot labeling performed using identical procedures. Bar, 5 μm. (B) Diffusion of CFTR before (black) and after (gray) butyrate treatment. For reference the 50th percentile (Q_2) and 75th percentile (Q_3) values are indicated. (C) Representative trajectories and summary histograms of *D* and range (at 2 s) for CFTR-3HA expressed in MDCK cells stably transfected with GFP-CFTR and stimulated with butyrate to upregulate GFP-CFTR expression. (D) Representative trajectories and summary histograms (range at 2 s) of CFTR-3HA and GFP-CFTRct87 coexpressed in COS7 cells. Single particle tracking data were acquired at 10 fps.

not shown). Expression of GFP-CFTRct87 had similar effects on CFTR mobility in MDCK and BHK cell lines (Supplemental Video 7, showing adjacent BHK cells expressing and not expressing transiently transfected GFP-CFTRct87).

DISCUSSION

Our data show remarkable immobilization of individual CFTR molecules at the cell surface. Several lines of evidence indicate that interaction of the CFTR C terminus with the actin skeleton is largely responsible for this immobilization, as diagrammed in Figure 1A. CFTR mobility was increased by deletion or modification of its C terminus, disruption of the cell actin skeleton, or expression of a dominant-negative EBP50/NHERF1 protein that prevents CFTR–ezrin coupling. These data indicate significant CFTR C-terminal interactions in living cells and suggest that other interactions are of much lesser importance with regard to restricting CFTR membrane mobility. Another interesting observation was that cells have limited capacity to couple/immobilize CFTR, such that overexpression of full-length CFTR or its C terminus leads to a substantial pool of mobile CFTR that was uncoupled from the actin skeleton. In the cells studied here, CFTR expression was within the range of that in two cells lines that natively express CFTR. The implication of this finding is that studies in many CFTR-transfected cell models are unlikely to preserve native CFTR interactions, at least with regard to C-terminal coupling to actin via EBP50 and ezrin.

During the completion of this work, a study of CFTR mobility in transfected cells was published (Bates *et al*., 2006). By photobleaching and image correlation spectroscopy, 50–60% mobility for CFTR was reported with increased *D* and percentage of mobility after addition of a C-terminal tail to block PDZ interactions, largely in agreement with our previous data (Haggie *et al*., 2004). Bates *et al*. (2006) also reported transient confinement of a C-terminal-blocked CFTR by SPT; however, as discussed in reference to Figure 3, the conclusion regarding the existence of transient confinement zones is probably not valid. Also, their study did not consider effects of CFTR expression levels or the related issue of possible cell type differences in CFTR mobility.

The formation of a CFTR-containing protein complex at the plasma membrane has been proposed based largely on biochemical studies such as cross-linking and immunoprecipitation (Li and Naren, 2005; Guggino and Stanton, 2006). The study here provides direct in vivo evidence for such a CFTR complex that includes EBP50, ezrin, and actin. Although not investigated here, various other proteins may participate in the CFTR complex. As mentioned in the Introduction, the PDZ domain proteins EBP50/NHERF1, E3KARP/NHERF2, CAL, and CAP70 have also been demonstrated to interact with the C terminus of CFTR; both EBP50 and NHERF2 associate with ezrin and consequently actin (Hall *et al*., 1998; Short *et al*., 1998; Wang *et al*., 1998; Sun *et al*., 2000b; Wang *et al*., 2000; Bretscher *et al*., 2002; Cheng *et al*., 2002; Benharouga *et al*., 2003). Regulatory proteins, including protein kinase A (Huang *et al*., 2000; Sun *et al*., 2000a), protein kinase C (Liedtke *et al*., 2002), the AMP-activated protein kinase (Hallows *et al*., 2000), protein phosphatases 2A (Thelin *et al*., 2005) and 2C (Zhu *et al*., 1999), and syntaxin 1A (Naren *et al*., 1997), also interact directly or indirectly with CFTR, as do membrane proteins, including the β2-adrenergic receptor (Naren *et al*., 2003) and the ROMK (Kir 1.1) K^+ channel (Yoo *et al*., 2004). Because the majority of these CFTR interactions have been demonstrated biochemically, interactions are generally characterized in dilute, nonphysiological solutions by using protein domains, and they are not quantified in terms of dissociation constants or the degree of association. Our data here indicate the presence of a CFTR multimolecular complex in living cells expressing relevant concentration of the various constituents of the complex, which is predominantly mediated by C-terminal interactions. The lack of jasplakinolide effect on CFTR-Δ26 diffusion confirmed that the majority of CFTR interactions with the actin cytoskeleton are mediated through its C terminus. Complexation of CFTR into a supramolecular assembly did not depend on protein phosphorylation, indicating that CFTR complex formation is constitutive rather than regulated by channel activation. Also, although C-terminal deletions of CFTR significantly increased its mobility, no alteration in protein kinase A-stimulated channel activity function was found, indicating that complex formation with the cytoskeleton is not necessary for channel phosphorylation (Benharouga *et al*., 2003; Ostedgaard *et al*., 2003).

Naturally occurring deletions at the carboxy terminus of CFTR (including Δ26 and Δ70) manifest varying clinical severity, with longer deletions (>70 amino acids) generally causing more severe disease (Cystic Fibrosis Genetic Con-

sortium Database, University of Toronto, Toronto, Ontario, Canada). The stability of CFTR with long carboxy-terminal deletions (e.g., CFTRΔ70) is greatly reduced in comparison with wild-type or Δ26 CFTR (Haardt *et al.*, 1999; Benharouga *et al.*, 2001; Ostedgaard *et al.*, 2003; Sharma *et al.*, 2004), suggesting that physical complexation of CFTR, mediated by carboxy-terminal amino acids, is not involved in CFTR stability.

Single particle tracking has been used to define the mobility of receptors expressed in excitatory and inhibitory neurons. Labeled receptors have been tracked using both transmission microscopy (e.g., 500-nm-diameter latex beads) and fluorescence techniques (e.g., antibodies conjugated to organic fluorophores such as Cy5 or linked to Qdots; Dahan *et al.*, 2003). Receptors such as the glycine receptor (GlyR), the metabotropic glutamate receptor (mGluR5), the α-amino-3-hydroxy-5-methyl-4-isoxazole propionic acid (AMPA) receptor and the *N*-methyl-D-aspartate receptor all show periods of high (0.02–0.12 $\mu m^2/s$) and low (0–0.01 $\mu m^2/s$) diffusion, with low diffusion being spatially correlated with synaptic regions (Choquet and Triller, 2002). Direct comparison of results obtained for receptors labeled with strategies using either Qdots or antibodies/Fab fragments labeled with organic fluorophores indicate that Qdots can faithfully report receptor diffusion, unless receptors diffuse into regions of geometric confinement such as synaptic clefts (Dahan *et al.*, 2003; Groc *et al.*, 2004). Contextually, receptors in neurons are similar to CFTR in terms of having multiple PDZ-type interactions and indirect association with the cytoskeleton (Choquet and Triller, 2002). However, whereas nearly all CFTR molecules are nearly immobile, the GlyR, mGluR5, and AMPA receptors alternate between diffusive and nondiffusive behaviors. As such, PDZ interactions in neurons do not consistently tether proteins, whereas the interaction of CFTR with PDZ domain proteins must be extremely stable.

Tracking of quantum dot-labeled membrane transport and receptor proteins has significant advantages over ensemble-averaged approaches, including photobleaching and fluorescence correlation spectroscopy, or tracking of membrane proteins after labeling with GFP or chemical probes. Single particle tracking yields spatial trajectories with nanometer spatial resolution and millisecond time resolution of large numbers of individual proteins, permitting characterization of complex and anomalous diffusive processes (Choquet and Triller, 2002; Kusumi *et al.*, 2005). The excellent brightness and photostability of quantum dots allows tracking over many minutes (Dahan *et al.*, 2003; Michalet *et al.*, 2005). In our experiments, nonspecific binding was ~1–2%, whereas nonspecific binding with latex beads applied to cells with laser tweezers or 40-nm colloidal gold particles is typically 15–30% or more (Sergé *et al.*, 2002; Suzuki *et al.*, 2005). Our experimental strategy was to use widefield fluorescence microscopy (as opposed to total internal reflection or confocal fluorescence microscopy), permitting detection of Qdots over a wide region of the cell apical membrane surface where CFTR is expressed. Single particle tracking of quantum dot-labeled CFTR may be possible to define in vivo CFTR interactions in native tissues derived from transgenic mice expressing epitope-tagged CFTRs or by using derivative of high-affinity CFTR inhibitors that bind at its external pore (Muanprasat *et al.*, 2004).

ACKNOWLEDGMENTS

We thank Adam D. Douglass and Dr. Ronald D. Vale (UCSF) and Dr. Erik R. Weeks (Emory University, Atlanta, GA) for assistance with trajectory analysis, and Dr. Walt Finkbeiner (UCSF) for providing HBE cultures. This study was supported by National Institutes of Health (NIH) Grants EB-00415, HL-73856, DK-72517, HL-59198, DK-35124, and EY13574; a Research Development Program grant from the Cystic Fibrosis Foundation (to A.S.V.); and grants from the Canadian Institute of Health Research and NIH (to G.L.L.).

REFERENCES

Bates, I. R., Hebert, B., Luo, Y., Liao, J., Bachir, A. I., Kolin, D. L., Wiseman, P. W., and Hanrahan, J. W. (2006). Membrane lateral diffusion and capture of CFTR within transient confinement zones. Biophys. J. *91*, 1046–1058.

Benharouga, M., Haardt, M., Kartner, N., and Lukacs, G. L. (2001). COOH-Terminal truncations promote proteasome-dependent degradation of mature cystic fibrosis transmebrane conductance regulator from post-Golgi compartments. J. Cell Biol. *153*, 957–970.

Benharouga, M., Sharma, M., So, J., Haardt, M., Drzymala, L., Popov, M., Schwapach, B., Grinstein, S., Du, K., and Lukacs, G. L. (2003). The role of the C terminus and Na^+/H^+ exchanger regulatory factor in the functional expression of cystic fibrosis transmembrane conductance regulator in nonpolarized cells and epithelia. J. Biol. Chem. *278*, 22079–22089.

Bertrand, C. A., and Frizzell, R. A. (2003). The role of regulated CFTR trafficking in epithelial secretions. Am. J. Physiol. *285*, C1–C18.

Bretscher, A., Edwards, K., and Fehon, R. G. (2002). ERM proteins and merlin, integrators at the cell cortex. Nat. Rev. Mol. Cell Biol. *3*, 586–599.

Cao, T. T., Deacon, H. W., Reczek, D., Bretscher, A., and von Zastrow, M. (1999). A kinase-regulated PDZ-interaction controls endocytic sorting of the β2-adrenergic receptor. Nature *401*, 286–290.

Cheng, J., Moyer, B. D., Milewski, H., Loffing, J., Ikeda, M., Mickle, J. E., Cutting, G. R., Li, M., Stanton, B. A., and Guggino, W. B. (2002). A Golgi-associated PDZ domain protein modulates cystic fibrosis transmembrane regulator plasma membrane expression. J. Biol. Chem. *277*, 3520–3529.

Choquet, D., and Triller, A. (2002). The role of receptor diffusion in the organization of the postsynaptic membrane. Nat. Rev. Neurol. *4*, 251–265.

Dahan, M., Levi, S., Luccardini, C., Rostaing, P., Riveau, B., and Triller, A. (2003). Diffusion dynamics of glycine receptors revealed by single-quantum dot tracking. Science *302*, 442–445.

Fujiwara, T., Ritchie, K., Murakoshi, H., Jacobson, K., and Kusumi, A. (2002). Phospholipids undergo hop diffusion in compartmentalized cell membrane. J. Cell Biol. *157*, 1071–1081.

Groc, L., Heine, M., Cognet, L., Brickley, K., Stephenson, F. A., Lounis, B., and Choquet, D. (2004). Differential activity-dependent regulation of the lateral mobilities of AMPA and NMDA receptors. Nat. Neurosci. *7*, 695–696.

Guggino, W. B., and Stanton, B. A. (2006). New insights into cystic fibrosis: molecular switches that regulate CFTR. Nat. Rev. Mol. Cell Biol. *7*, 426–436.

Haardt, M., Benharouga, M., Lechardeur, D., Kartner, N., and Lukacs, G. L. (1999). C-Terminal truncations destabilize the cystic fibrosis transmembrane conductance regulator without impairing its biogenesis. J. Biol. Chem. *274*, 21873–21877.

Haggie, P., Stanton, B. A., and Verkman, A. S. (2004). Increased diffusional mobility of CFTR at the plasma membrane after deletion of its C-terminal PDZ binding motif. J. Biol. Chem. *279*, 5494–5500.

Hall, R. A., Ostedgaard, L. S., Premont, R. T., Blitzer, J. T., Rahman, N., Welsh, M. J., and Lefkowitz, R. J. (1998). A C-terminal motif found in the β_2-adrenergic receptor, P2Y1 receptor and cystic fibrosis transmembrane conductance regulator determines binding to the Na^+/H^+ exchanger regulatory factor family of PDZ proteins. Proc. Natl. Acad. Sci. USA *95*, 8496–8501.

Hallows, K. R., Raghuram, V., Kemp, B. E., Witters, L. A., and Foskett, J. K. (2000). Inhibition of cystic fibrosis transmembrane conductance regulator by novel interactions with the metabolic sensor AMP-activated protein kinase. J. Clin. Investig. *105*, 1711–1721.

Huang, P., Trotter, K., Boucher, R. C., Milgram, S. L., and Stutts, M. J. (2000). PKA holoenzyme is functionally coupled to CFTR by AKAPs. Am. J. Physiol. *278*, C417–C422.

Kusumi, A., Nakada, C., Ritchie, K., Murase, K., Suzuki, K., Murakoshi, H., Kasai, R. S., Kondo, J., and Fujiwara, T. (2005). Paradigm shift of the plasma membrane concept from the two-dimensional continuum fluid to the partitioned fluid: high-speed single-molecule tracking of membrane molecules. Annu. Rev. Biophys. Biomol. Struct. *34*, 351–378.

Li, C., and Naren, A. P. (2005). Macromolecular complexes of cystic fibrosis transmembrane conductance regulator and its interacting partners. Pharmacol. Ther. *108*, 208–233.

Liedtke, C. M., Yun, C.H.C., Kyle, N., and Wang, D. (2002). Protein kinase Cε-dependent regulation of cystic fibrosis transmembrane regulator involves

binding to a receptor for activated C kinase (RACK1) and RACK1 binding to Na^+/H^+ exchange regulatory factor. J. Biol. Chem. *277*, 22925–22933.

Michalet, X., Pinaud, F. F., Bentolila, L. A., Tsay, J. M., Doose, S., Li, J. J., Sundaresan, G., Wu, A. M., Gambhir, S. S., and Weiss, S. (2005). Quantum dots for live cells, in vivo imaging and diagnostics. Science *307*, 538–544.

Moyer, B. D., *et al*. (1999a). A PDZ-interacting domain in CFTR is an apical membrane polarization signal. J. Clin. Invest. *104*, 1353–1361.

Moyer, B. D., *et al*. (2000). The PDZ-interacting domain of cystic fibrosis transmembrane conductance regulator is required for functional expression in the apical plasma membrane. J. Biol. Chem. *275*, 27069–27074.

Moyer, B. D., Loffing-Cueni, D., Loffing, J., Reynolds, D., and Stanton, B. A. (1999b). Butyrate increases apical membrane CFTR but reduces chloride secretion in MDCK cells. Am. J. Physiol. *277*, F271–F276.

Muanprasat, C., Sonawane, N. D., Salinas, D., Taddei, A., Galietta, L. J., and Verkman, A. S. (2004). Discovery of glycine hydrazide pore-occluding CFTR inhibitors: mechanism, structure-activity analysis, and in vivo efficacy. J. Gen. Physiol. *124*, 109–113.

Naren, A. P., Cobb, B., Li, C.-J., Roy, K., Nelson, D., Heda, G. D., Liao, J., Kirk, K. L., Sorscher, E. J., Hanrahan, J. W., and Clancy, J. P. (2003). A macromolecular complex of β_2 adrenergic receptor, CFTR and ezrin/radixin/moesin-binding phosphoprotein 50 is regulated by PKA. Proc. Natl. Acad. Sci. USA *100*, 342–346.

Naren, A. P., Nelson, D., Xie, W., Jovov, B., Pevsner, J., Bennet, M. K., Benos, D. J., Quick, M. W., and Kirk, K. L. (1997). Regulation of CFTR chloride channels by syntaxin and Munc18 isoforms. Nature *390*, 302–305.

Okamoto, K.-I., Nagai, T., Miyawaki, A., and Hayashi, Y. (2004). Rapid and persistent modulation of actin dynamics regulates postsynaptic reorganization underlying bidirectional plasticity. Nat. Neurosci. *7*, 1104–1112.

Ostedgaard, L. S., Randak, C., Rokhlina, T., Karp, P. H., Vermeer, D., Excoffon, K.J.A., and Welsh, M. J. (2003). Effects of C-terminal deletions on cystic fibrosis transmembrane conductance regulator function in cystic fibrosis airway epithelia. Proc. Natl. Acad. Sci. USA *100*, 1937–1942.

Pedemonte, N., Lukacs, G. L., Du, K., Caci, E., Zegarra-Moran, O., Galietta, L. J., and Verkman, A. S. (2005). Small-molecule correctors of defective ΔF508-CFTR cellular processing identified by high-throughput screening. J. Clin. Investig. *115*, 2564–2571.

Prince, L. S., Peter, K., Hatton, S. R., Zaliauskiene, L., Cotlin, L. F., Clancy, J. P., Marchase, R. B., and Collawn, J. F. (1999). Efficient endocytosis of the cystic fibrosis transmembrane conductance regulator requires a tyrosine-based signal. J. Biol. Chem. *274*, 3602–3609.

Raghuram, V., Hormouth, H., and Foskett, J. K. (2003). A kinase-regulated mechanism controls CFTR channel gating by disrupting bivalent PDZ domain interactions. Proc. Natl. Acad. Sci. USA *100*, 9620–9625.

Raghuram, V., Mak, D.-O.D., and Foskett, J. K. (2001). Regulation of cystic fibrosis transmembrane conductance regulator single-channel gating by bivalent PDZ-domain-mediated interactions. Proc. Natl. Acad. Sci. USA *98*, 1300–1305.

Saxton, M. J. (1997). Single-particle tracking: the distribution of diffusion coefficients. Biophys. J. *72*, 1744–1753.

Sergé, A., Fourgeaud, L., Hémar, A., and Choquet, D. (2002). Receptor activation and Homer differentially control the lateral mobility of metabotropic glutamate receptor 5 in the neuronal membrane. J. Neuro. *22*, 3910–3920.

Sharma, M., *et al*. (2004). Misfolding diverts CFTR from recycling to degradation; quality control at early endosomes. J. Cell Biol. *164*, 923–933.

Shelly, M., Mosesson, Y., Citri, A., Lavi, S., Zwang, Y., Melamed-Book, N., Aroeti, B., and Yarden, Y. (2003). Polar expression of ErbB-2/HER2 in epithelia; bimodal regulation by Lin-7. Dev. Cell *5*, 475–486.

Short, D. B., Trotter, K. W., Reczek, D., Kreda, S. M., Bretscher, A., Boucher, R. C., Stutts, M. J., and Milgram, S. L. (1998). An apical PDZ protein anchors the cystic fibrosis transmembrane conductance regulator to the cytoskeleton. J. Biol. Chem. *273*, 19797–19801.

Sun, F., Hug, M. J., Bradbury, N. A., and Frizzell, R. A. (2000a). Protein kinase A associates with cystic fibrosis transmembrane conductance regulator via an interaction with ezrin. J. Biol. Chem. *275*, 14360–14366.

Sun, F., Hug, M. J., Lewarchik, C. M., Yun, C. H., Bradbury, N. A., and Frizzell, R. A. (2000b). E3KARP mediates the association of ezrin and protein kinase A with the cystic fibrosis transmembrane conductance regulator in airway cells. J. Biol. Chem. *275*, 29539–29546.

Suzuki, K., Ritchie, K., Kajikawa, E., Fujiwara, T., and Kusumi, A. (2005). Rapid hop diffusion of a G-protein-coupled receptor in the plasma membrane as revealed by single-molecule techniques. Biophys. J. *88*, 3659–3680.

Swiatecka-Urban, A., Duhaime, M., Coutermarsh, B., Karlson, K. H., Collawn, J., Milewski, H., Cutting, G. R., Guggino, W. B., Langford, G., and Stanton, B. A. (2002). PDZ domain interaction controls the endocytic recycling of the cystic fibrosis transmembrane conductance regulator. J. Biol. Chem. *277*, 40099–40105.

Thelin, W. R., Kesimer, M., Tarran, R., Kreda, S. M., Grubb, B. R., Sheehan, J. K., Stutts, M. J., and Milgram, S. L. (2005). CFTR is regulated by a direct interaction with the protein phosphatase PP2A. J. Biol. Chem. *280*, 41512–41520.

Wang, S., Raab, R. W., Schatz, P. J., Guggino, W. B., and Li, M. (1998). Peptide binding consensus of the NHE-RF-PDZ1 domain matches the C-terminal sequence of cystic fibrosis transmembrane conductance regulator (CFTR). FEBS Lett. *427*, 103–108.

Wang, S., Yue, H., Derin, R. B., Guggino, W. B., and Li, M. (2000). Accessory protein facilitated CFTR-CFTR interaction, a molecular mechanism to potentiate the chloride channel activity. Cell *103*, 169–179.

Weinman, E. J., Steplock, D., Wang, Y., and Shenolikar, S. (1995). Characterization of a protein cofactor that mediates protein kinase A regulation of the renal brush border membrane Na^+/H^+ exchanger. J. Clin. Investig. *95*, 2143–2149.

Widdicombe, J. H., Sachs, L. A., and Finkbeiner, W. E. (2003). Effects of growth surface on differentiation of cultures of human tracheal epithelium. In Vitro Cell Dev. Biol. Anim. *39*, 51–55.

Yoo, D., Flagg, T. P., Olsen, O., Raghuram, V., Foskett, J. K., and Welling, P. A. (2004). Assembly and trafficking of a multiprotein ROMK (Kir 1.1) channel complex by PDZ interactions. J. Biol. Chem. *279*, 6863–6873.

Zhu, T., Dahan, D., Evagelidis, A., Zheng, S., Luo, J., and Hanrahan, J. W. (1999). Association of cystic fibrosis transmembrane conductance regulator and protein phosphatase 2C. J. Biol. Chem. *274*, 29102–29107.